Photonic crystal enhanced silicon cell based thermophotovoltaic systems

Yi Xiang Yeng,[1,2,*] **Walker R. Chan,**[1,2] **Veronika Rinnerbauer,**[4] **Veronika Stelmakh,**[1,2] **Jay J. Senkevich,**[2] **John D. Joannopoulos,**[1,2,3] **Marin Soljačić,**[1,2,3] **and Ivan Čelanović**[2]

[1]*Research Laboratory of Electronics, Massachusetts Institute of Technology, Cambridge, Massachusetts 02139, USA*
[2]*Institute of Soldier Nanotechnologies, Massachusetts Institute of Technology, Cambridge, Massachusetts 02139, USA*
[3]*Department of Physics, Massachusetts Institute of Technology, Cambridge, Massachusetts 02139, USA*
[4]*Johannes Kepler University, Institute of Semiconductor and Solid State Physics, Altenbergerstraße 69, 4040 Linz, Austria*

[*]*yxyeng@mit.edu*

Abstract: We report the design, optimization, and experimental results of large area commercial silicon solar cell based thermophotovoltaic (TPV) energy conversion systems. Using global non-linear optimization tools, we demonstrate theoretically a maximum radiative heat-to-electricity efficiency of 6.4% and a corresponding output electrical power density of $0.39\,\mathrm{W\,cm^{-2}}$ at temperature $T = 1660\,\mathrm{K}$ when implementing both the optimized two-dimensional (2D) tantalum photonic crystal (PhC) selective emitter, and the optimized 1D tantalum pentoxide – silicon dioxide PhC cold-side selective filter. In addition, we have developed an experimental large area TPV test setup that enables accurate measurement of radiative heat-to-electricity efficiency for any emitter-filter-TPV cell combination of interest. In fact, the experimental results match extremely well with predictions of our numerical models. Our experimental setup achieved a maximum output electrical power density of $0.10\,\mathrm{W\,cm^{-2}}$ and radiative heat-to-electricity efficiency of 1.18% at $T = 1380\,\mathrm{K}$ using commercial wafer size back-contacted silicon solar cells.

OCIS codes: (350.4238) Nanophotonics and photonic crystals; (260.2160) Energy transfer; (290.6815) Thermal emission; Thermophotovoltaics; Selective emitters/absorbers.

References and links

1. B. D. Wedlockt, "Thermo-Photo-Voltaic energy conversion," Proc. IEEE **51**, 694–698 (1963).
2. T. J. Coutts, "A review of progress in thermophotovoltaic generation of electricity," Renew. Sust. Energ. Rev. **3**, 77–184 (1999).
3. M. Zenker, A. Heinzel, G. Stollwerck, J. Ferber, and J. Luther, "Efficiency and power density potential of combustion-driven thermophotovoltaic systems using GaSb photovoltaic cells," IEEE Trans. Electron. Dev. **48**, 367–376 (2001).
4. W. E. Horne, M. D. Morgan, V. S. Sundaram, and T. Butcher, "500 Watt Diesel Fueled TPV Portable Power Supply," AIP Conf. Proc. **653**, 91–100 (2003).
5. C. S. Murray, C. J. Crowley, S. Murray, N. A. Elkouh, R. W. Hill, and D. E. Chubb, "Thermophotovoltaic converter design for radioisotope power systems," in 6th Thermophotovoltaic Generation of Electricity Conference (AIP, 2004), pp. 123–132.

#226352 - $15.00 USD Received 6 Nov 2014; accepted 6 Jan 2015; published 30 Jan 2015

6. C. J. Crowley, N. A. Elkouh, S. Murray, and D. L. Chubb, "Thermophotovoltaic converter performance for radioisotope power systems," in Space Technology and Applications International Forum (AIP, 2005), pp. 601–614.
7. R. W. Kaszeta, Y. X. Yeng, M. Ghebrebrhan, J. D. Joannopoulos, M. Soljačić, and I. Celanovic, "Advanced radiative emitters for radioisotope thermophotovoltaic power systems," in 5th World Conference on Photovoltaic Energy Conversion / Ninth Thermophotovoltaic World Conference (2010).
8. N. P. Harder and P. Wurfel, "Theoretical limits of thermophotovoltaic solar energy conversion," Semicond. Sci. Technol. **18**, S151–S157 (2003).
9. V. M. Andreev, A. S. Vlasov, V. P. Khvostikov, O. A. Khvostikova, P. Y. Gazaryan, S. V. Sorokina, and N. A. Sadchikov, "Solar thermophotovoltaic converters based on tungsten emitters," J. Sol. Ener. Eng. **129**, 298–303 (2007).
10. A. Lenert, D. M. Bierman, Y. Nam, W. R. Chan, I. Celanović, M. Soljačić, and E. N. Wang, "A nanophotonic solar thermophotovoltaic device," Nat. Nanotechnol. **9**, 126–130 (2014).
11. W. Yang, S. Chou, C. Shu, H. Xue, and Z. Li, "Design, Fabrication, and Testing of a Prototype Microthermophotovoltaic System," J. Microelectromech. Syst. **13**, 851–856 (2004).
12. L. M. Fraas and L. Minkin, "TPV history from 1990 to present & future trends," AIP Conf. Proc. **890**, 17–23 (2007).
13. B. Wernsman, R. R. Siergiej, S. D. Link, R. G. Mahorter, M. N. Palmisiano, R. J. Wehrer, R. W. Schultz, G. P. Schmuck, R. L. Messham, S. Murray, C. S. Murray, F. Newman, D. Taylor, D. M. Depoy, and T. Rahmlow, "Greater than 20% radiant heat conversion efficiency of a thermophotovoltaic radiator/module system using reflective spectral control," IEEE Trans. Electron. Dev. **51**, 512–515 (2004).
14. W. R. Chan, P. Bermel, R. C. N. Pilawa-Podgurski, C. H. Marton, K. F. Jensen, J. J. Senkevich, J. D. Joannopoulos, M. Soljačić, and I. Celanovic, "Toward high-energy-density, high-efficiency, and moderate-temperature chip-scale thermophotovoltaics." Proc. Natl. Acad. Sci. USA **110**, 5309–14 (2013).
15. R. N. Bracewell and R. M. Swanson, "Silicon photovoltaic cells in thermophotovoltaic conversion," Electric Power Research Institute Report, ER-633 (1978).
16. K. Qiu and a. Hayden, "Development of a silicon concentrator solar cell based TPV power system," Energ. Convers. Manage. **47**, 365–376 (2006).
17. B. Bitnar, W. Durisch, and R. Holzner, "Thermophotovoltaics on the move to applications," Appl. Energ. **105**, 430–438 (2013).
18. L. Ferguson and F. Dogan, "A highly efficient NiO-Doped MgO matched emitter for thermophotovoltaic energy conversion," Mat. Sci. Eng. B **83**, 35–41 (2001).
19. B. Bitnar, W. Durisch, J.-C. Mayor, H. Sigg, and H. Tschudi, "Characterisation of rare earth selective emitters for thermophotovoltaic applications," Sol. Energy Mater. Sol. Cells **73**, 221–234 (2002).
20. A. Narayanaswamy and G. Chen, "Thermal emission control with one-dimensional metallodielectric photonic crystals," Phys. Rev. B **70**, 125101 (2004).
21. D. L. C. Chan, M. Soljačić, and J. D. Joannopoulos, "Thermal emission and design in one-dimensional periodic metallic photonic crystal slabs," Phys. Rev. E **74**, 16609 (2006).
22. M. U. Pralle, N. Moelders, M. P. McNeal, I. Puscasu, A. C. Greenwald, J. T. Daly, E. A. Johnson, T. George, D. S. Choi, I. El-Kady, and R. Biswas, "Photonic crystal enhanced narrow-band infrared emitters," Appl. Phys. Lett. **81**, 4685–4687 (2002).
23. H. Sai and H. Yugami, "Thermophotovoltaic generation with selective radiators based on tungsten surface gratings," Appl. Phys. Lett. **85**, 3399–3401 (2004).
24. R. Biswas, D. Zhou, I. Puscasu, E. Johnson, A. Taylor, and W. Zhao, "Sharp thermal emission and absorption from conformally coated metallic photonic crystal with triangular lattice," Appl. Phys. Lett. **93**, 063307 (2008).
25. J. G. Fleming, S. Y. Lin, I. El-Kady, R. Biswas, and K. M. Ho, "All-metallic three-dimensional photonic crystals with a large infrared bandgap," Nature **417**, 52–55 (2002).
26. S. Y. Lin, J. Moreno, and J. G. Fleming, "Three-dimensional photonic-crystal emitter for thermal photovoltaic power generation," Appl. Phys. Lett. **83**, 380–382 (2003).
27. T. A. Walsh, J. A. Bur, Y.-S. Kim, T.-M. Lu, and S. Y. Lin, "High-temperature metal coating for modification of photonic band edge position," J. Opt. Soc. Am. B **26**, 1450–1455 (2009).
28. M. Ghebrebrhan, P. Bermel, Y. X. Yeng, J. D. Joannopoulos, M. Soljačić, and I. Celanovic, "Tailoring thermal emission via Q-matching of photonic crystal resonances," Phys. Rev. A **83**, 033810 (2011).
29. Y. X. Yeng, W. R. Chan, V. Rinnerbauer, J. D. Joannopoulos, M. Soljačić, and I. Celanovic, "Performance analysis of experimentally viable photonic crystal enhanced thermophotovoltaic systems," Opt. Express **21**, A1035–A1051 (2013).
30. V. Rinnerbauer, S. Ndao, Y. X. Yeng, J. J. Senkevich, K. F. Jensen, J. D. Joannopoulos, M. Soljacic?, I. Celanovic, and R. D. Geil, "Large-area fabrication of high aspect ratio tantalum photonic crystals for high-temperature selective emitters," J. Vac. Sci. Technol. B **31**, 011802 (2013).
31. V. Rinnerbauer, Y. X. Yeng, W. R. Chan, J. J. Senkevich, J. D. Joannopoulos, M. Soljačić, and I. Celanovic, "High-temperature stability and selective thermal emission of polycrystalline tantalum photonic crystals," Opt. Express **21**, 11482–11491 (2013).

#226352 - $15.00 USD Received 6 Nov 2014; accepted 6 Jan 2015; published 30 Jan 2015

32. V. Liu and S. Fan, "A free electromagnetic solver for layered periodic structures," Comput. Phys. Comm. **183**, 2233–2244 (2012).
33. A. F. Oskooi, D. Roundy, M. Ibanescu, P. Bermel, J. Joannopoulos, and S. G. Johnson, "Meep: A flexible free-software package for electromagnetic simulations by the FDTD method," Comput. Phys. Comm. **181**, 687–702 (2010).
34. S. G. Johnson, "The NLopt nonlinear-optimization package," http://ab-initio.mit.edu/nlopt.
35. J. Zhao, A. Wang, P. P. Altermatt, S. R. Wenham, and M. A. Green, "24% Efficient perl silicon solar cell: Recent improvements in high efficiency silicon cell research," Sol. Energy Mater. Sol. Cells **42**, 87–99 (1996).
36. R. T. Kristensen, J. F. Beausang, and D. M. Depoy, "Frequency selective surfaces as near-infrared electromagnetic filters for thermophotovoltaic spectral control," J. Appl. Phys. **95**, 4845–4851 (2004).
37. F. O'Sullivan, I. Celanovic, N. Jovanovic, J. Kassakian, S. Akiyama, and K. Wada, "Optical characteristics of one-dimensional Si/SiO_2 photonic crystals for thermophotovoltaic applications," J. Appl. Phys. **97**, 033529 (2005).
38. T. D. Rahmlow, D. M. Depoy, P. M. Fourspring, H. Ehsani, J. E. Lazo-Wasem, and E. J. Gratrix, "Development of front surface, spectral control filters with greater temperature stability for thermophotovoltaic energy conversion," in 7th Thermophotovoltaic Generation of Electricity Conference (AIP, 2007), pp. 59–67.
39. R. K. Huang, C. A. Wang, M. K. Connors, G. W. Turner, and M. W. Dashiell, "Hybrid back surface reflector GaInAsSb thermophotovoltaic devices," AIP Conf. Proc. **738**, 329–336 (2004).
40. L. B. Karlina, M. M. Kulagina, N. K. Timoshina, A. S. Vlasov, and V. M. Andreev, "$In_{0.53}Ga_{0.47}As$/InP conventional and inverted thermophotovoltaic cells with back surface reflector," AIP Conf. Proc. **890**, 182–189 (2007).
41. P. Wilkinson, "Photonic Bloch oscillations and Wannier-Stark ladders in exponentially chirped Bragg gratings," Phys. Rev. E **65**, 056616 (2002).
42. H. R. Philipp, "The infrared optical properties of SiO_2 and SiO_2 layers on silicon," J. Appl. Phys. **50**, 1053–1057 (1979).
43. G. A. Al-Jumaily and S. M. Edlou, "Optical properties of tantalum pentoxide coatings deposited using ion beam processes," Thin Solid Films **209**, 223–229 (1992).
44. A. V. Tikhonravov, M. K. Trubetskov, and G. W. Debell, "Application of the needle optimization technique to the design of optical coatings." Appl. Opt. **35**, 5493–508 (1996).
45. NREL, "Best research-cell efficiencies chart," http://www.nrel.gov/ncpv/images/efficiency_chart.jpg.

1. Introduction

In thermophotovoltaic (TPV) energy conversion systems, direct conversion of thermal radiation to electricity is achieved via the photovoltaic (PV) effect [1, 2]. TPV energy conversion offers many advantages, including the promise of highly versatile, modular, and compact high power density energy conversion systems that have no moving parts, leading to quiet and robust operation. In addition, virtually any high grade heat source can be used, including waste heat [2], fossil fuels [3, 4], radioisotopes [5–7], and solar energy [8–10]. Compared to conventional solar PV conversion, the heat source is significantly closer to the PV cell, resulting in photon flux and power density that are orders of magnitude higher. However, due to the much lower temperatures achievable in practical TPV systems ($T < 2000\,\mathrm{K}$), the majority of emitted photons lie in the near- to mid-infrared (IR) spectrum, hence it is widely acknowledged that the path to higher TPV efficiencies lies in the development of low bandgap TPV cells. In fact, many TPV system experimental efforts have been reported for gallium antimonide (GaSb) [4, 9, 11, 12], indium gallium arsenide (InGaAs) [5, 6, 13], and indium gallium arsenide antimonide (InGaAsSb) cells [10, 14]. In contrast, efforts to utilize silicon (Si) cells for TPV energy conversion systems have been virtually non-existent as the larger energy gap of Si demands higher operating temperatures for efficient energy conversion. However, the application of Si PV cells is interesting as they are abundant, cheap, and commercially available in large sizes. In addition, the technology is significantly more mature and closer to theoretical limits compared to low bandgap TPV cells.

To the best of our knowledge, only three experimental efforts have been reported to-date for Si cell based TPV (Si-TPV): Bracewell and Swanson reported a TPV efficiency of 10% (does not include cavity losses) with specially designed p-i-n Si cells and a blackbody cavity emitter at $T = 2350\,\mathrm{K}$ [15]; Qiu *et al.* reported an output power density of $0.2\,\mathrm{W\,cm^{-2}}$ using Sunpower solar cells specially designed for low solar concentrations and an ytterbia (Yb_2O_3) rare-earth

#226352 - $15.00 USD Received 6 Nov 2014; accepted 6 Jan 2015; published 30 Jan 2015

selective emitter [16]; Bitnar *et al.* reported an overall fuel-to-electricity efficiency of 3.96% and a corresponding output electrical power density of $0.104\,\mathrm{W\,cm^{-2}}$ using solar cells developed by the University of New South Wales (UNSW) and a Yb_2O_3 rare-earth selective emitter at $T > 1700\,\mathrm{K}$ [17]. However, in all of these investigations, direct measurements of radiative heat-to-electricity efficiency that include cavity losses were not performed; this is vital in order to understand the main loss mechanisms in TPV energy conversion systems. Additionally, lower temperatures ($T \approx 1500\,\mathrm{K}$) are more practical given the difficulties of engineering systems that are reliable over long time scales at high temperatures. In this investigation, we propose a combination of optimized two-dimensional (2D) metallic PhC selective emitters and 1D PhC based cold-side dielectric filters that will enable reasonable performance at lower temperatures. We will first discuss the methods used to obtain optimized designs of both the selective emitter and the selective filter. Performance predictions using a realistic TPV system level numerical model will then be presented. Following that, the experimental setup used to validate the numerical models as well as the measurements obtained will be discussed, before presenting our concluding remarks.

2. Design and optimization

2.1. Selective emitter: 2D metallic photonic crystals

The primary challenge of designing Si-TPV systems for a lower $T = 1500\,\mathrm{K}$ lies in the small fraction of energy that is potentially convertible due to Si possessing a high energy gap ($E_g = 1.12\,\mathrm{eV}$). For a greybody with emittance $\varepsilon = 0.9$, only 2.8% of the radiative energy is convertible. The remaining non-convertible photons emitted result in parasitic heat losses, which would also lead to highly undesirable elevated PV cell operating temperatures. Efficient spectral control is thus a necessity. Spectral control can be achieved firstly via the use of selective emitters to preferentially emit convertible photons. To date, various selective emitters have been investigated; from rare-earth oxides [18,19], to 1D [20,21], 2D [22–24], and 3D PhCs [25–27]. Here, we select the 2D tantalum (Ta) PhC as the selective emitter as this design offers a sharp emittance cutoff that is easily shifted and optimized [28,29], is scalable to large areas [30], and has been proven to be thermally stable at high temperatures in high vacuum conditions [31]. The 2D Ta PhC consists of a square array of cylindrical holes with radius r, depth d, and period a etched onto an optically smooth Ta surface as shown in the inset of Fig. 1.

Rigorous coupled wave analysis (RCWA) methods [32] were used to obtain the reflectance of the 2D Ta PhCs at all angles of incidence, which allows us to infer the hemispherical emittance via Kirchoff's law. The Lorentz–Drude model of Ta fitted to elevated temperature ($T \sim 1500\,\mathrm{K}$) emittance [31] was used to capture the optical dispersion of Ta in the simulations. To ensure accuracy, the number of Fourier expansion orders were doubled until the results converged. We have also confirmed that simulations using conventional finite-difference time-domain (FDTD) methods [33] agree very well with RCWA formulations based on both polarization decomposition and normalized vector basis when more than 320 Fourier expansion orders are used.

Optimized designs of 2D Ta PhCs can be easily obtained using the formalism outlined in Ref. 29. The global optimization routines were implemented via NLOpt, a free software packaged developed at MIT that allows comparison between various global optimization algorithms [34]. The following figure of merit was used for the optimization:

$$\mathrm{FOM} = x\eta_{\mathrm{TPV}} + (1-x)\frac{J_{\mathrm{elec}}^{\mathrm{PhC}}}{J_{\mathrm{elec}}^{\mathrm{BB}}} \tag{1}$$

where η_{TPV} is the radiative heat-to-electricity efficiency of the TPV system, which is the ratio of output electrical power density to the net radiant exitance of the emitter (model includes effects of multiple reflections and reabsorption events, as well as cavity losses), $J_{\mathrm{elec}}^{\mathrm{PhC}}/J_{\mathrm{elec}}^{\mathrm{BB}}$ captures the

#226352 - $15.00 USD Received 6 Nov 2014; accepted 6 Jan 2015; published 30 Jan 2015

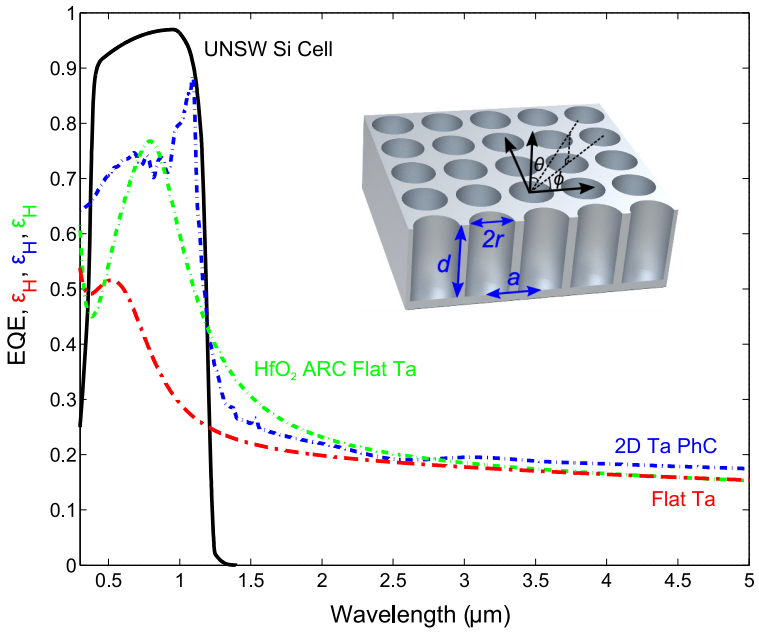

Fig. 1. Spectral hemispherical emittance ε_{H} (at temperature T = 1500 K) of the optimized 2D tantalum photonic crystal (2D Ta PhC: r = 0.28 μm, d = 2.20 μm, a = 0.61 μm) shows excellent match with the external quantum efficiency (EQE) of the University of New South Wales's (UNSW) silicon (Si) solar cells [35]. An optimized 85 nm anti-reflection coating of hafnium oxide on top of flat Ta (HfO_2 ARC Flat Ta) is a simple alternative that also performs reasonably well.

output electrical power density performance of the 2D Ta PhC emitter compared to a blackbody, and $x \in [0,1]$ is the weighting given to η_{TPV} in the optimization routine, which could be modified depending on design goals. In this investigation, we are mainly concerned in obtaining the highest η_{TPV} possible, thus $x = 0.9$ was used. For simulation and optimization purposes, we used Si cell data published by UNSW [35]. Using this, the optimized 2D Ta PhC design for our target operating temperature of $T = 1500$ K was obtained. As can be seen in Fig. 1, the emittance shows excellent match with the external quantum efficiency (EQE) of the UNSW Si cells. Figure 1 also shows the emittance of flat Ta with an optimized 85 nm anti-reflection coating of hafnium oxide (HfO_2 ARC Flat Ta), which is an easily fabricated alternative. η_{TPV} and J_{elec} for all three selective emitters in an Si-TPV system with T = 1500 K and view factor $F = 0.99$ (achievable with 100 mm × 100 mm flat plate geometry with $s = 500$ μm) are shown in Table 1. As can be seen, the optimized 2D Ta PhC selective emitter enables greater than 100% improvement in η_{TPV} over the greybody emitter ($\varepsilon = 0.9$), while still maintaining high $J_{\mathrm{elec}}^{\mathrm{PhC}} / J_{\mathrm{elec}}^{\mathrm{BB}}$ of 0.76.

2.2. *Cold-side selective filter: 1D dielectric photonic crystals*

Another spectral control approach relies on recuperating non-convertible photons using front surface reflectors [36–38] and back surface reflectors [39, 40] on the PV cell. In this investigation, we consider a simple, experimentally realizable solution based on a variant of the quarter-wave stack 1D PhC: the exponentially chirped distributed Bragg reflector (DBR) [41]. It is essentially a periodic quarter-wave stack with an exponentially varying period, such that

#226352 - $15.00 USD
Received 6 Nov 2014; accepted 6 Jan 2015; published 30 Jan 2015

Table 1. Comparison of radiative heat-to-electricity efficiency η_{TPV} and output electrical power density J_{elec} between a greybody emitter (ε = 0.9), optimized HfO_2 ARC Flat Ta, and optimized 2D Ta PhC (r = 0.28 μm, d = 2.20 μm, a = 0.61 μm) in UNSW Si cell based thermophotovoltaic (Si-TPV) systems at T = 1500 K with view factor $F = 0.99$ (achievable with 100 mm × 100 mm flat plate geometry with emitter-TPV cell separation of 500 μm).

Emitter	η_{TPV} (%)	J_{elec} (W/cm^2)
Greybody (ε = 0.9)	1.93	0.238
Optimized HfO_2 ARC Flat Ta	3.48	0.173
Optimized 2D Ta PhC	4.12	0.210

the effective stop band is broadened. The period of the l-th stack is given by:

$$a_l = a_0 \exp(lB) \tag{2}$$

where a_0 is the period of the first stack, and B is the exponential chirp factor given by:

$$B = \frac{1}{l} \ln\left(\frac{1+b}{1-b}\right) \tag{3}$$

where b is defined as the relative range such that:

$$a_l = a_0 \frac{1+b}{1-b} \tag{4}$$

The first stack is chosen such that it corresponds to a standard quarter-wave stack:

$$a_0 = \frac{\lambda_c}{4n_1} + \frac{\lambda_c}{4n_2} \tag{5}$$

where λ_c is related to the cutoff wavelength of the filter, and n_1 and n_2 are respectively the refractive index of the first and second dielectric material. As per the standard quarter-wave stack, the larger the refractive index contrast, the better the performance of the filter. From Eqs. (2) and (5), we can see that only two parameters (λ_c and b) define the exponentially chirped DBR, and thus the optical properties. Again, we used NLOpt to determine the optimum values for maximum FOM defined as follows:

$$\text{FOM} = x\eta_{\text{spec}} + (1-x)\eta_{\text{emit}} \tag{6}$$

where η_{spec} and η_{emit} are respectively the spectral efficiency and emission efficiency given by:

$$\eta_{\text{spec}} = \frac{\int_0^{\lambda_c} i_{\text{BB}}(\lambda,T)\,\varepsilon_{\text{H}}(\lambda)\,R_{\text{H}}(\lambda)\,\mathrm{d}\lambda}{\int_0^{\infty} i_{\text{BB}}(\lambda,T)\,\varepsilon_{\text{H}}(\lambda)\,R_{\text{H}}(\lambda)\,\mathrm{d}\lambda} \tag{7}$$

$$\eta_{\text{emit}} = \frac{\int_0^{\lambda_c} i_{\text{BB}}(\lambda,T)\,\varepsilon_{\text{H}}(\lambda)\,R_{\text{H}}(\lambda)\,\mathrm{d}\lambda}{\int_0^{\lambda_c} i_{\text{BB}}(\lambda,T)\,\mathrm{d}\lambda} \tag{8}$$

where $i_{\text{BB}}(\lambda,T)$ is the spectral radiance of a blackbody, $\varepsilon_{\text{H}}(\lambda)$ is the spectral hemispherical emittance of the selective emitter, and $R_{\text{H}}(\lambda)$ is the spectral hemispherical reflectance of the filter. η_{spec} captures the fraction of convertible energy, while η_{emit} is the ratio of convertible power of the emitter–filter combination to that of a blackbody. $\eta_{\text{spec}} = \eta_{\text{emit}} = 1$ represents the

#226352 - $15.00 USD Received 6 Nov 2014; accepted 6 Jan 2015; published 30 Jan 2015

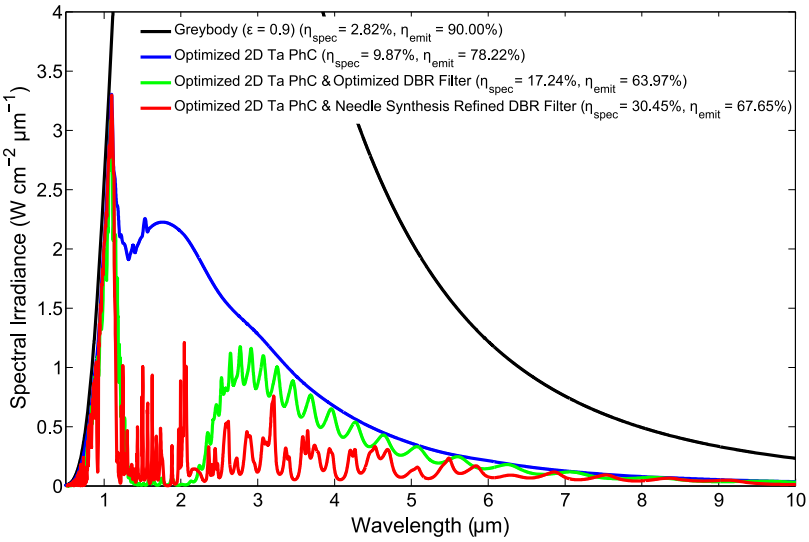

Fig. 2. Effective spectral irradiance incident on photovoltaic (PV) cell for various selective emitter and cold-side filter combinations of interest at $T = 1500\,\mathrm{K}$.

limit of performance desired. Again, the weighting factor x can be tailored to give either more emphasis to efficiency or power density.

In this investigation, we choose tantalum pentoxide (Ta_2O_5) and silicon dioxide (SiO_2) with n of approximately 2.1 and 1.5 respectively; they are both highly transparent in the wavelength range $0.25\,\mu\mathrm{m} < \lambda < 5.0\,\mu\mathrm{m}$, and are industry standard optical coatings [42, 43]. To ensure practical realization, we consider only 30 bilayers for the filter design. Using NLOpt with $x = 0.15$, the optimum DBR filter was determined to have $\lambda_c = 1.397\,\mu\mathrm{m}$ and $b = 0.211$. When combined with the optimized 2D Ta PhC, this filter enables an improvement of approximately 511% and 75% in η_{spec} compared to respectively the greybody ($\varepsilon = 0.9$) and optimized 2D Ta PhC based TPV system without the filter, albeit at a slightly reduced η_{emit}. The improvement is clearly seen in Fig. 2, whereby the effective spectral irradiance incident on the PV cell for $1.1\,\mu\mathrm{m} < \lambda < 2.3\,\mu\mathrm{m}$ is mostly suppressed, i.e. reflected back to the emitter.

The optimized exponentially chirped DBR filter can further be improved via the needle synthesis optimization method [44]. This algorithm is, in essence, a perturbative method. In this case, the original optimized exponentially chirped DBR filter was repeatedly modified via the addition or subtraction of a thin layer of material ($\approx 10\,\mathrm{nm}$ to $20\,\mathrm{nm}$) at a location which results in the greatest improvement in the FOM. The process was repeated until the FOM ceases to improve. By applying this on the optimized exponentially chirped DBR filter, a further 77% improvement in η_{spec} is seen when coupled with the optimized 2D Ta PhC selective emitter. As can be seen in Fig. 2, the needle synthesis method improves on the original optimized exponentially chirped DBR filter by further reducing effective spectral irradiance incident on the PV cell for $\lambda > 2.3\,\mu\mathrm{m}$, albeit at a smaller penalty of allowing a small number of photons through for $1.1\,\mu\mathrm{m} < \lambda < 2.3\,\mu\mathrm{m}$.

2.3. Thermophotovotaic system performance

Using the numerical model described in Ref. 29, estimates of η_{TPV} using UNSW Si PV cells and various emitter–filter combinations in $F = 0.99$ TPV systems were obtained; the results are illustrated in Fig. 3. As T increases, η_{TPV} decreases primarily due to series resistance under

#226352 - $15.00 USD Received 6 Nov 2014; accepted 6 Jan 2015; published 30 Jan 2015

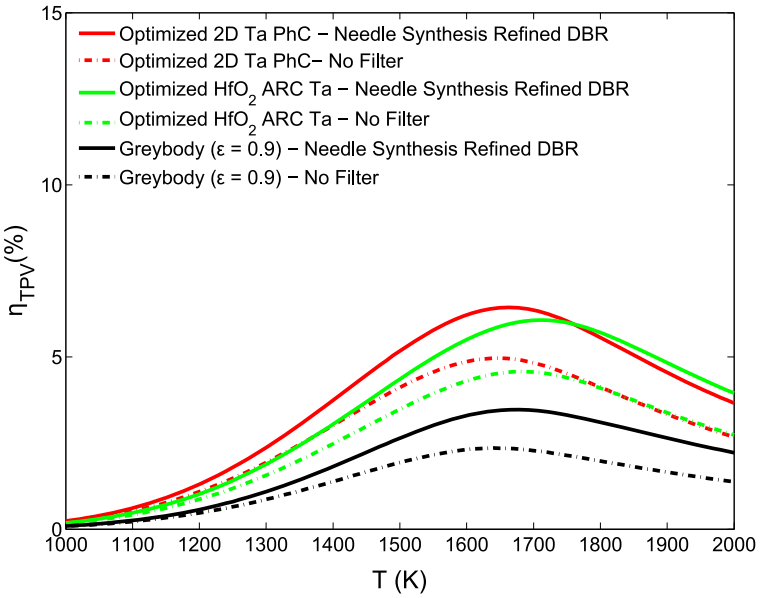

Fig. 3. η_{TPV} as a function of T for various selective emitter and cold-side filter combinations of interest in Si-TPV systems with $F = 0.99$.

high current injection, which is $\gtrsim 5$ times of that under standard AM1.5 solar irradiance. Thus, specially designed Si cells for low solar concentrations ($C = 5$–20) would be more suitable for TPV applications.

For the greybody ($\varepsilon = 0.9$), maximum radiative heat-to-electricity efficiency $\eta_{\text{TPV, max}}$ of 2.35% is achieved at T = 1640 K. By replacing the greybody with the optimized HfO_2 ARC Ta or optimized 2D Ta PhC selective emitter, $\eta_{\text{TPV, max}}$ can be increased to 4.58% (at T = 1680 K) and 4.97% (at T = 1650 K) respectively. The highest $\eta_{\text{TPV, max}}$ of 6.44% (at T = 1660 K) is achieved with the optimized 2D Ta PhC and needle synthesis refined DBR filter combination. In this investigation, the target operating T is 1500 K; η_{TPV} and J_{elec} at $T = 1500$ K for various emitter and cold-side filter combinations of interest are shown in Table 2.

Table 2. Comparison of η_{TPV} and J_{elec} between a greybody emitter (ε = 0.9), flat Ta, optimized HfO_2 ARC flat Ta (85nm of HfO_2 on top of flat Ta), and optimized 2D Ta PhC (r = 0.28 μm, d = 2.20 μm, a = 0.61 μm) at T = 1500 K with or without the needle synthesis refined DBR filter in $F = 0.99$ Si-TPV systems.

Emitter	Filter	η_{TPV} (%)	J_{elec} (W/cm^2)
Greybody (ε = 0.9)	N/A	1.93	0.24
Flat Ta	N/A	2.17	0.09
Optimized HfO_2 ARC Ta	N/A	3.48	0.17
Optimized 2D Ta PhC	N/A	4.12	0.21
Greybody (ε = 0.9)	Needle Synthesis Refined DBR	2.64	0.22
Flat Ta	Needle Synthesis Refined DBR	2.63	0.08
Optimized HfO_2 ARC Ta	Needle Synthesis Refined DBR	4.36	0.15
Optimized 2D Ta PhC	Needle Synthesis Refined DBR	5.17	0.19

#226352 - $15.00 USD
Received 6 Nov 2014; accepted 6 Jan 2015; published 30 Jan 2015

3. Experimental method and results

3.1. Solar cell packaging

In this investigation, we used state-of-the-art Sunpower solar cells, which are to-date the most efficient commercially available Si PV cells boasting a solar-to-electricity efficiency of 25.6% [45]. One of the key reasons for superior efficiencies of Sunpower Si cells is the back-contacted design, i.e. all electrical connections are located at the back of the solar cell, thus eliminating shading losses that plague conventional front-contacted designs. For the particular cell we were using, 6 terminals (3 +ve and 3 -ve) of the size of 7.5 mm $\times$ 7.5 mm are provided for electrical connections. All other areas need to be free of electrical connections to ensure no electrical shorts exists. Concurrently, for efficient TPV energy conversion, it is important to ensure that the Sunpower Si cell is in good thermal contact with the heat sink. In order to achieve both precisely placed electrical connections and excellent thermal path elsewhere, the Sunpower Si cell was mounted on top of a Bergquist HPL Thermal Clad. It is, in essence, similar to a printed circuit board, of which electrical connections are provided by copper (Cu) foils, while the remaining area is covered with a thin layer (38 μm thick) of high thermal conductivity ($\kappa = 3.0\,\mathrm{W\,m^{-1}\,K^{-1}}$) dielectric material, all on top of a 1 mm thick Cu substrate. To adhere the Sunpower Si cell to the Bergquist HPL Thermal Clad, a layer of 3M 8805 thermally conductive ($\kappa = 0.60\,\mathrm{W\,m^{-1}\,K^{-1}}$) electrically insulating pressure sensitive tape (125 μm thick) was used at areas requiring electrical insulation, while a small amount of electrically conducting silver-filled grease (AREMCO Heat-Away 641-EV) was applied on electrical contacts. Since the Bergquist HPL Thermal Clad is not perfectly flat, it was bonded onto a thicker (10 mm) aluminum (Al) substrate with Epotek's H74 thermally conductive epoxy ($\kappa = 1.25\,\mathrm{W\,m^{-1}\,K^{-1}}$). A thin layer of thermal grease (AREMCO Heat-Away 641-EV, $\kappa = 5.58\,\mathrm{W\,m^{-1}\,K^{-1}}$) was then applied between the Al substrate and the heat sink. The bolting force coupled with the thicker and thus stiffer Al substrate ensures good thermal contact with the heat sink. Using this, we were able to cool the Sunpower Si cells to room temperature.

3.2. Thermophotovoltaic cavity design

The key parameters that we desire to measure are η_{TPV} and output electrical power P_{elec}. In order to measure η_{TPV}, a precise calorimetric approach to accurately measure the net radiant power emitted P_{rad} is necessary. This was achieved in the experimental setup shown in Fig. 4, which was specifically designed to accurately account for all energy transfers in the system; input electrical power P_{in} to the heater (100 mm diameter HeatWave Labs 1200 °C UHV Heater) and P_{elec} of the PV cell were measured simply using accurate voltage and current meters (Fluke 289 True RMS Meter, Fluke i310s Current Clamp); measurement of the parasitic conductive heat loss P_{cond} was performed by monitoring the temperature difference of the bottom Al posts using two high-accuracy 100Ω Class A DIN Platinum 3-wire resistance temperature detectors (RTD); parasitic radiative heat loss of the Cu radiation shields were neglected since they are at much lower temperatures of $\lesssim 500$ K, thus contributing $\lesssim 3\%$ of the overall energy balance (in fact, ignoring this results in a more conservative measurement of η_{TPV}, albeit at an acceptably small error). η_{TPV} is then given by:

$$\eta_{\mathrm{TPV}} = \frac{P_{\mathrm{elec}}}{P_{\mathrm{rad}}} = \frac{P_{\mathrm{elec}}}{P_{\mathrm{in}} - P_{\mathrm{cond}}} \tag{9}$$

3.3. Thermophotovoltaic system measurements

In this investigation, we are focused on obtaining experimental results using just the optimized HfO_2 ARC flat Ta emitter. This serves as a vital preliminary experimental investigation, and more importantly allows us to verify the numerical models presented in Ref. 29, before deciding

#226352 - $15.00 USD Received 6 Nov 2014; accepted 6 Jan 2015; published 30 Jan 2015

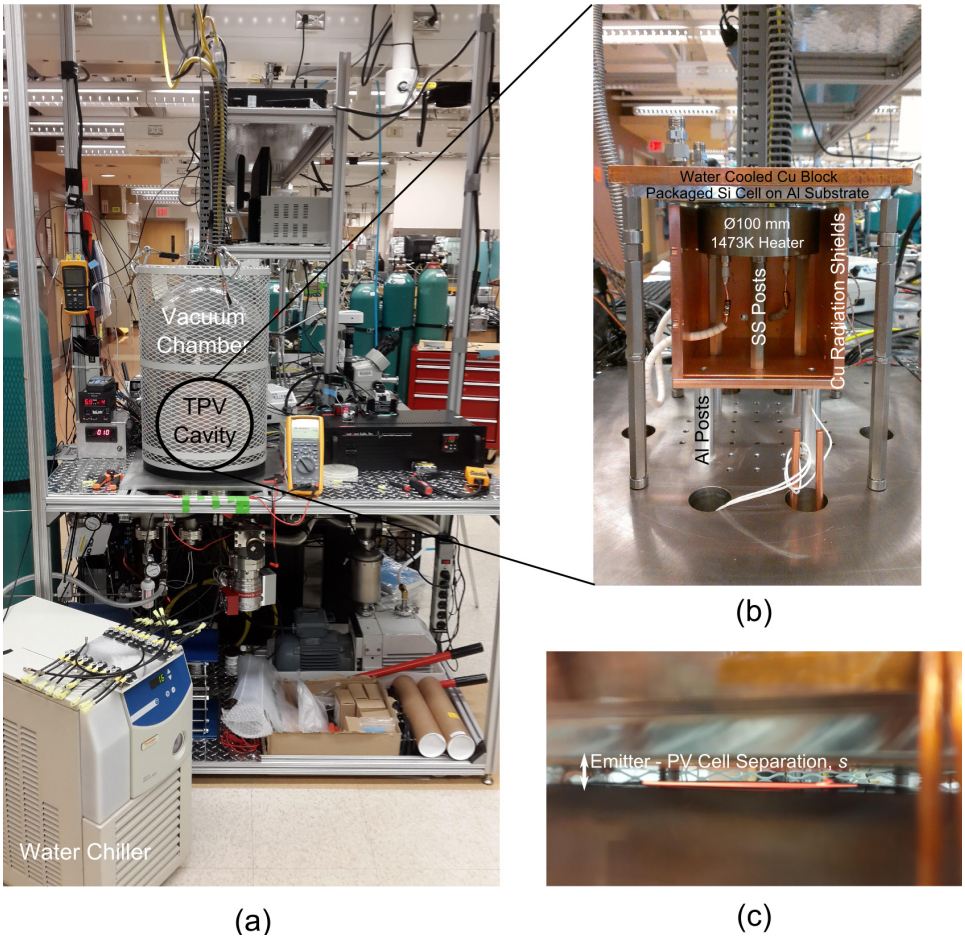

Fig. 4. (a) Entire TPV efficiency measurement setup. (b) Close-up view of TPV cavity design. SS denotes stainless steel. (c) Close-up view of glowing emitter during operation at 1473 K.

to undertake significant efforts toward realizing large area 2D Ta PhCs, and fabrication and implementation of the needle synthesis refined DBR filter, both of which require efforts beyond the scope of this publication.

Stock flat 2.5 mm thick Ta sputtering targets of 100 mm diameter and were sourced from Shanghai Jiangxi Metals Co. The flat Ta wafer was then polished to a mean surface roughness of ≈ 5.94 Å and surface flatness of ≈ 5.0 µm. The polished Ta wafer was then deposited with 85 nm of HfO_2 using atomic layer deposition (Cambridge Nanotech Savannah 200). The thickness and refractive index of the HfO_2 coating was verified using an ellipsometer (J. A. Woollam Co. M2000). In addition, ε of the HfO_2 ARC Flat Ta measured indirectly using the FTIR (Nexus 870) reflectance accessory (PIKE Technologies VeeMAX II) with a known standard Al mirror (Thorlabs) was found to match extremely well with numerical predictions.

Accurate measurements of the top surface temperature of the emitter are of extreme importance, without which inhibits comparison of experimental data to numerical models. Here, we spot welded type K thermocouples on top of the emitter. Since the area of the weld covers $\lesssim$ 0.01% of the total area of the emitter, it is safe to assume that the perturbation is small, and thus

#226352 - $15.00 USD Received 6 Nov 2014; accepted 6 Jan 2015; published 30 Jan 2015

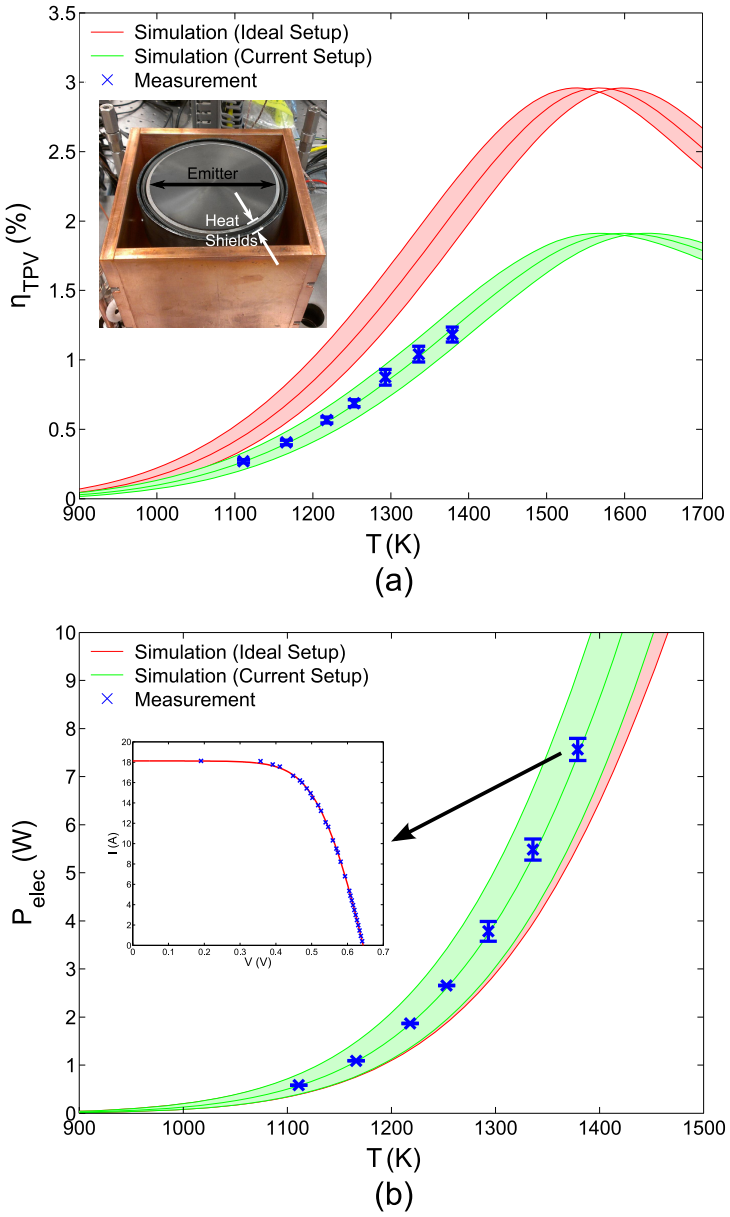

Fig. 5. Measured (a) η_{TPV} and (b) P_{elec} as a function of T using Sunpower Si cell with optimized 85 nm thick HfO_2 ARC coating on flat Ta with emitter-PV cell separation $s =$ 2.0 mm. The simulation results are represented as bands to account for an arbitrary temperature uncertainty of $\pm$ 30 K. Inset of (a) shows top view of 100 mm diameter HeatWave Labs 1200 °C UHV Heater. The heat shields are estimated to be $\approx$ 250 K cooler than the top surface of the emitter; this resulted in significant parasitic radiative heat loss absorbed by the PV cell, which negatively affects η_{TPV} as shown by the green curve (the 'Current Setup'). The 'Ideal Setup' simulations were performed without effects of the heat shields, i.e. only radiation from the emitter is considered. Inset of (b) shows the Sunpower Si cell IV curve measurement at the heater's maximum temperature rating.

#226352 - $15.00 USD
Received 6 Nov 2014; accepted 6 Jan 2015; published 30 Jan 2015

this method is a reasonably accurate measurement of the top surface temperature. Indeed, the experimentally measured P_{elec} shown in Fig. 5(b) with emitter-PV cell separation $s = 2.0\,mm$ shows excellent agreement with simulations. Highest recorded P_{elec} = 7.6 W and $\eta_{TPV} = 1.18\%$ was obtained at $T = 1380\,K$; at this point the heater internals were at $T = 1500\,K$, which is the heater's maximum temperature rating, and thus higher temperatures are unattainable with this setup.

However, note that measured η_{TPV}'s are $\approx 50\%$ of numerical model predictions denoted by *Ideal Setup* in Fig. 5(a). In the *Ideal Setup* numerical simulations, the heater is assumed to only comprise of the selective emitter with diameter of 100 mm. However, as can be seen in the inset of Fig. 5(a), there are heat shields that contribute to the effective size of the heater such that the measured diameter is 118 mm, and more significantly 28% of the effective area is covered by the heat shields. The inner and outer heat shields comprise of inconel and stainless steel respectively. In fact, by including the area of the heat shields in simulations assuming reasonable parameters of $\varepsilon = 0.9$ and $T \approx 250\,K$ cooler than the selective emitter top surface for the heat shields, we obtained simulation results that match extremely well with the experimental results as indicated by *Current Setup* numerical predictions in Fig. 5. As seen in Fig. 5(b), the heat shields contribute no P_{elec} due to lower temperatures, but result in an increase in net radiative power absorbed by the PV cell by $\approx 80\%$ compared to just the selective emitter alone.

4. Conclusions

In summary, we have investigated Si PV cells for TPV applications as they are inexpensive and commercially available in large sizes, and the technology is significantly more mature and closer to theoretical limits compared to low bandgap TPV cells. Using global non-linear optimization tools, we have demonstrated theoretically a maximum radiant heat-to-electricity efficiency η_{TPV} of 6.4% and output electrical power density $J_{elec} = 0.4\,W\,cm^{-2}$ at $T = 1660\,K$ when implementing both the optimized 2D Ta PhC selective emitter, and the needle synthesis refined DBR cold-side selective filter.

In addition, we have developed an experimental large area TPV test setup that enables accurate measurement of η_{TPV} for any emitter-filter-TPV cell combination of interest. Our experimental setup achieved a maximum electrical power output P_{elec} of 7.6 W and η_{TPV} of 1.18% at $T = 1380\,K$ using standard wafer size back-contacted Sunpower solar cells. The experimental results agree extremely well with numerical predictions.

Acknowledgments

This work is partially supported by the Army Research Office through the Institute for Soldier Nanotechnologies under Contract No. W911NF-13-D-0001. Y. X. Y., W. R. C., V. S., and M. S. are partially supported by the Solid-State Solar-Thermal Energy Conversion Center (S3TEC) Energy Research Frontier Center (EFRC) of the Department of Energy under Grant No. DE-SC0001299. V. R. gratefully acknowledges funding by the Austrian Science Fund (FWF): J3161-N20.